THE JOURNAL OF PHYSICAL CHEMISTRY B

Article

pubs.acs.org/JPCB

Desorption Kinetics of Benzene and Cyclohexane from a Graphene Surface

R. Scott Smith* and Bruce D. Kay*

Physical and Computational Sciences Directorate, Pacific Northwest National Laboratory, Richland, Washington 99352, United States

ABSTRACT: The desorption kinetics for benzene and cyclohexane from a graphene covered Pt(111) surface were investigated using temperature-programmed desorption (TPD). The benzene desorption spectra show well-resolved monolayer and multilayer desorption peaks. The benzene monolayer and submonolayer TPD spectra for coverages greater than ~0.1 ML have nearly the same desorption peak temperature and have line shapes which are consistent with first-order desorption kinetics. For benzene coverages greater than 1 ML, the TPD spectra align on a common leading edge which is consistent with zero-order desorption. An "inversion" procedure in which the prefactor is varied to find the value that best reproduces the entire set of experimental desorption spectra was used to analyze the benzene data. The inversion analysis of the benzene TPD spectra yielded a desorption activation energy of 54 ± 3 kJ/mol with a prefactor of $10^{17\pm1}$ s^{-1}. The TPD spectra for cyclohexane also have well-resolved monolayer and multilayer desorption features. The desorption leading edges for the monolayer and the multilayer TPD spectra are aligned indicating zero-order desorption kinetics in both cases. An Arrhenius analysis of the monolayer cyclohexane TPD spectra yielded a desorption activation energy of 53.5 ± 2 kJ/mol with a prefactor of $10^{16\pm1}$ ML s^{-1}.

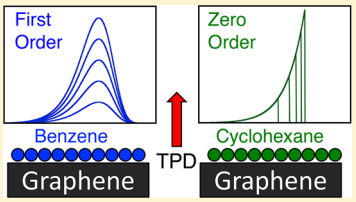

INTRODUCTION

The interactions of adsorbates with graphene is of interest in a variety of fields including catalysis,[1−5] material science,[6,7] and electronics.[8−11] In addition, theoreticians have studied adsorbate-graphene interactions as models to improve the calculation of weakly bound and van der Waals systems.[12−19] Understanding the interactions and desorption kinetics from carbon-based substrates is also important for astrophysicists to create models for the composition of various astrophysical bodies (e.g., comets, interplanetary ices, interplanetary dust, and planetary surfaces).[20−28]

Recently, we have used graphene covered Pt(111) as an analog for carbonaceous surfaces to study the desorption of some astrophysically relevant adsorbates.[29,30] The desorption spectra for all of the adsorbates studied (water, methanol, ethanol, Ar, Kr, Xe, N_2, O_2, CO, methane, ethane, and propane) have well-resolved monolayer and multilayer desorption peaks. Further, the leading edges for both the monolayer and multilayer desorption peaks are aligned on a common curve which is a signature of the zero-order desorption. These results contrasted with studies on highly oriented pyrolytic graphite (HOPG) which had reported the observation of fractional-order desorption kinetics for monolayer coverages of water, methanol, and ethanol.[22,23,27] The difference between these results could be due to several experimental factors including the dosing (background versus molecular beam) and detection (background versus line-of-sight).[29]

In the present article we study the desorption kinetics of benzene and cyclohexane from a graphene covered Pt(111) surface. The interaction of benzene with graphene has been used as a model system for calculating $\pi-\pi$ interactions which are believed to be important in biological systems (e.g., protein and DNA structure).[13,14,17−19,31] Compared with the number of theory papers, there have been relatively few experimental studies. Zacharia et al.[32] and Ulbrict et al.[33] have studied benzene desorption from HOPG (graphite) and Burghaus et al.[34,35] have studied benzene desorption from graphene on metal and SiO_2 supports. In these prior works the experimental desorption results are analyzed using the Redhead equation.[36] This equation uses the desorption peak temperature and an assumed or estimated prefactor to estimate adsorbate binding energies. In the present work, we use an "inversion" procedure in which the prefactor is varied to find the value that best reproduces the entire set of experimental desorption spectra. The value of prefactor will affect the calculated binding energy. Here we use molecular beam dosing techniques to acquire high quality desorption spectra that are analyzed with the inversion procedure to obtain accurate binding energies and prefactors. We find that while the binding energies for benzene and cyclohexane are nearly the same, the desorption order for the two species are different.

EXPERIMENTAL SECTION

The graphene layer was grown by exposing a Pt(111) substrate held at 1100 K to a molecular beam of decane. This procedure has been shown to produce an single layer of carbon that has the structure of graphite.[37] The sample substrate was mounted within an ultrahigh vacuum system (UHV) described in detail previously.[38,39] The 1 cm diameter Pt(111) crystal was cooled

Special Issue: Miquel B. Salmeron Festschrift

Received: May 25, 2017
Revised: July 3, 2017
Published: July 5, 2017

DOI: 10.1021/acs.jpcb.7b05102
J. Phys. Chem. B 2018, 122, 587−594

by a closed-cycle helium cryostat to a base temperature of ~25 K and was resistively heated through two tantalum leads spot-welded on the back. A K-type thermocouple spot-welded to the back of the sample measured the temperature with a precision of better than ±0.01 K and was calibrated to an absolute accuracy of better than ±2 K utilizing the desorption of Kr and H_2O multilayers. Benzene and cyclohexane were deposited at 25 K and at normal incidence using a quasi-effusive molecular beam collimated by four stages of differential pumping. The beams for both species were created by expanding 1.0 Torr of the vapor through a 1 mm diameter orifice. The vapor pressure and flow were controlled by a leak valve. Experiments were also performed at a deposition temperature of 100 K (not shown) and the desorption results were essentially identical. For each species, a ML was defined as the dose needed to saturate the monolayer desorption peak. The dosing beam fluxes were 0.11 ML/s for benzene and 0.10 ML/s for cyclohexane. Temperature-programmed desorption (TPD) spectra were obtained using an Extrel quadrapole mass spectrometer in a line-of-sight configuration. A linear heating rate of 1 K/s was used for all the TPD experiments.

RESULTS AND DISCUSSION

Benzene and Cyclohexane Desorption from Graphene. The TPD spectra for benzene films deposited at 25 K on a graphene covered Pt(111) substrate and heated at 1.0 K/s are displayed in Figure 1. The desorption spectra for coverages from 0.11 to 1.0 ML (blue curves) are displayed in Figure 1a. The TPD spectra have the same desorption peak temperature (for coverages greater than 0.11 ML) and are not aligned on the leading or trailing edges. These features and the asymmetric line shapes are characteristic of first-order desorption. Figure 1b displays benzene desorption spectra from both the first layer (blue) and the second layer (1.11 to 2.0 ML, red). In this case, the leading edges from the second layer are aligned and give rise to a peak that is well-separated from the first layer peak. The alignment of the leading edges is characteristic of zero-order desorption.

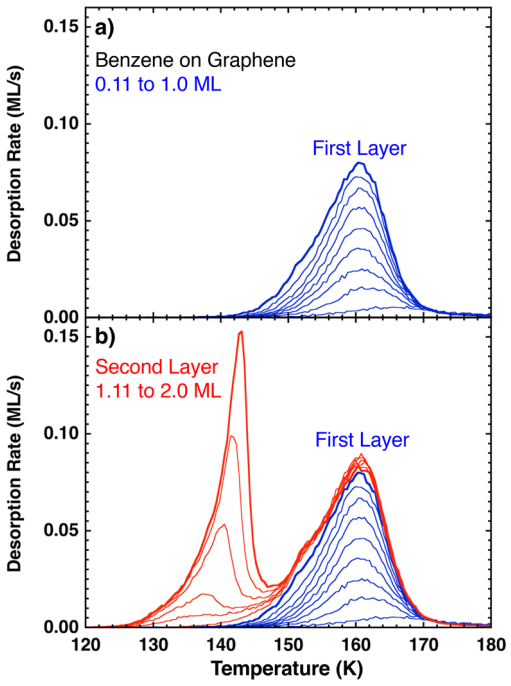

Figure 1. TPD spectra for benzene deposited on a graphene covered Pt(111) substrate at 25 K and heated at 1.0 K/s. (a) Benzene TPD spectra for monolayer coverages of 0.11, 0.22, 0.33, 0.44, 0.55, 0.66, 0.77, 0.88, and 1.0 ML (blue). (b) Benzene TPD spectra for second layer coverages of 1.11, 1.22, 1.33, 1.55, 1.77, and 2.0 ML (red) plotted along with those for the monolayer (blue).

Figure 2 displays the TPD spectra for cyclohexane films deposited at 25 K on a graphene covered Pt(111) substrate and heated at 1.0 K/s. The top panel, Figure 2a, displays the monolayer (0.1 to 1 ML, blue) spectra and the bottom panel, Figure 2b, displays both the monolayer and second layer (1.1 to 2.0 ML, red) spectra. The leading edges for both the first and second layer desorption spectra are aligned indicating zero-order desorption kinetics. Zero-order desorption kinetics for submonolayer coverages can occur if an equilibrium is established between individual adsorbates and adsorbate islands on a time scale that is fast compared to the desorption rate.[40−42] The situation is analogous to the equilibrium between the vapor (isolated adsorbate) and the condensed phase (islands). The establishment of a two-dimensional, two-phase coexistence defines the chemical potential and thus the vapor pressure of the system. If during the desorption process this equilibrium is maintained, the desorption rate (vapor pressure) will depend only on temperature and not on coverage, i.e., the desorption kinetics are zero-order.

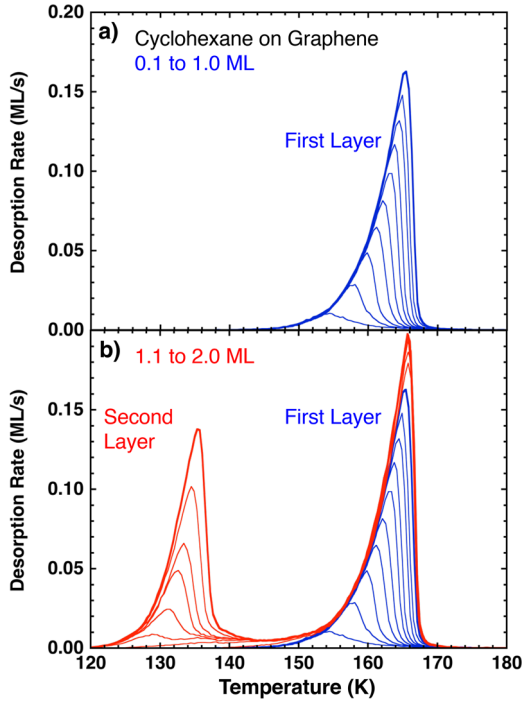

Figure 2. TPD spectra for cyclohexane deposited on a graphene covered Pt(111) substrate at 25 K and heated at 1.0 K/s. (a) Cyclohexane TPD spectra for monolayer coverages of 0.1, 0.2, 0.3, 0.4, 0.5, 0.6, 0.7, 0.8, 0.9, and 1.0 ML (blue). (b) Cyclohexane TPD spectra for second layer coverages of 1.1, 1.2, 1.3, 1.4, 1.5, 1.6, 1.8, and 2.0 ML (red) plotted along with those for monolayer and submonolayer coverages (blue).

Figure 3 displays multilayer (2 to 30 ML) TPD desorption spectra for benzene (Figure 3a) and cyclohexane (Figure 3b). The inset in Figure 3a is an enlargement of the desorption leading edge for benzene TPD spectra with 2, 2.5, and 3 ML. The inset shows that the 2 ML desorption rate is initially

DOI: 10.1021/acs.jpcb.7b05102
J. Phys. Chem. B 2018, 122, 587−594

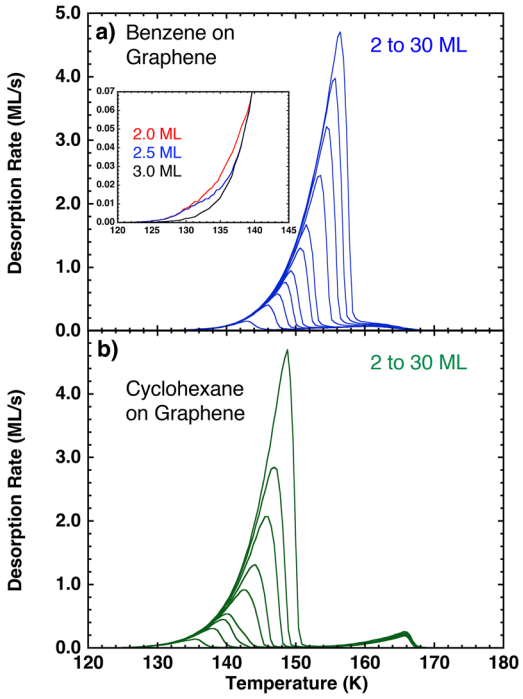

Figure 3. Multilayer TPD spectra for benzene and cyclohexane deposited on a graphene covered Pt(111) substrate at 25 K and heated at 1.0 K/s. (a) TPD spectra for benzene coverages of 2, 3, 4, 5, 6, 8,10, 15, 20, 25, and 30 ML. Inset: An enlargement of the leading edges for the 2, 2.5, and 3 ML TPD spectra. (b) TPD spectra for cyclohexane coverages of 2, 3, 4, 5, 7.5,10, 15, 20, and 30 ML.

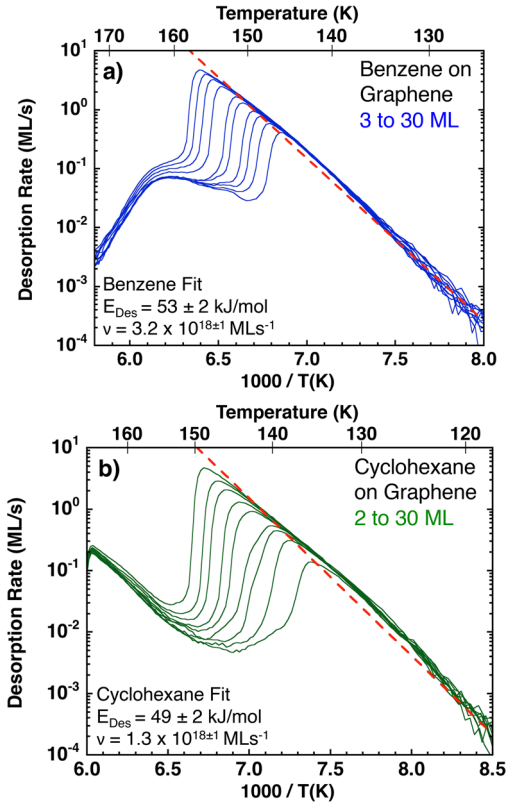

Figure 4. Arrhenius plot of the multilayer TPD spectra for benzene and cyclohexane from Figure 3. (a) TPD spectra for benzene coverages of 3, 4, 5, 6, 8,10, 15, 20, 25, and 30 ML. The dashed line is an Arrhenius fit to the 30 ML curve which yielded an activation energy of 53 ± 2 kJ/mol and a prefactor of $3.2 \times 10^{18\pm1}$ ML s^{-1}. (b) TPD spectra for cyclohexane coverages of 2, 3, 4, 5, 7.5,10, 15, 20, and 30 ML. The dashed line is an Arrhenius fit to the 30 ML curve which yielded an activation energy of 49 ± 2 kJ/mol and a prefactor of $1.3 \times 10^{18\pm1}$ ML s^{-1}.

greater than the 3 ML but at higher temperature (~140 K) the curves converge. The 2.5 ML spectrum behaves similarly except that it comes into alignment with the 3 ML curve at a slightly lower temperature (~137 K). For coverages above 3 ML the TPD spectra are aligned from the onset of measurable desorption. This behavior is typically an indication of a phase change in the film.[43] For example, films vapor deposited at low temperature often grow as amorphous solids and can crystallize when heated to a higher temperature. The transformation from the higher free energy amorphous phase to the lower free energy crystalline results in a decrease in desorption rate (vapor pressure). We have previously observed using infrared spectroscopy that amorphous benzene films readily crystallize at low temperatures.[44] The multilayer cyclohexane TPD spectra in Figure 3b are all aligned from the onset which means that there is no phase change during desorption. This could mean that the cyclohexane film had crystallized at a temperature before the onset of measurable desorption.

Figure 4 is an Arrhenius plot of the multilayer TPD spectra for benzene and cyclohexane from Figure 3. The dashed line in Figure 4a is an Arrhenius fit to the leading edge of the 30 ML benzene TPD spectrum which yielded an activation energy of 53 ± 2 kJ/mol and a prefactor of $3.2 \times 10^{18\pm1}$ ML s^{-1}. The dashed line in Figure 4b is an Arrhenius fit to the leading edge of the 30 ML cyclohexane TPD spectrum which yielded an activation energy 49 ± 2 kJ/mol and a prefactor of $1.3 \times 10^{18\pm1}$ ML s^{-1}.

The results for the desorption of benzene (Figure 1) and cyclohexane (Figure 2) clearly show that the desorption kinetics are different for the two. Determination of the desorption binding energies and prefactors will require different approaches.

Energetics of Benzene Desorption from Graphene—Inversion Analysis. In this section, we analyze the benzene monolayer TPD spectra in Figure 1 to extract the desorption parameters. Adsorbate desorption rates are mathematically expressed using the Polanyi–Wigner rate equation,

$$\frac{d\theta}{dT} = \frac{\nu\theta^n}{\beta}\exp^{-E_{Des}/RT} \quad (1)$$

where ν is the prefactor, θ is the coverage, n is the desorption order, β is the heating rate, R is the gas constant, and T is the temperature.[45] In eq 1, increasing E_{Des} results in a higher peak desorption temperature, T_{Peak}. Redhead developed a relationship between E_{Des} and T_{Peak} by taking the derivative of the desorption rate with respect to temperature, setting it equal to zero, and rearranging to get,

$$E_{Des} = RT_{Peak}\left[\ln\left(\frac{\nu T_{Peak}}{\beta}\right) - 3.64\right] \quad (2)$$

for first order desorption, $n = 1$.[36] Because of its simplicity, the Redhead eq (eq 2) is widely employed to obtain desorption energies, however it has several limitations. The first is that one must have a value for the prefactor, which is often assumed to be 10^{13} s^{-1}. However, this assumption can lead to errors for adsorbates where the real desorption prefactor is larger. Another limitation is that one obtains a single desorption

DOI: 10.1021/acs.jpcb.7b05102
J. Phys. Chem. B 2018, 122, 587–594

energy which does not take into account adsorbate−adsorbate interactions that may result in a coverage dependent activation energy.

Here we analyze the benzene desorption data using an "inversion" method.[30,39,46−50] In this method the Polanyi−Wigner rate eq (eq 1) is rearranged to give,

$$E_{\mathrm{Des}}(\theta) = -RT\ln\left(\frac{\beta\frac{d\theta}{dT}}{\nu\theta}\right) \tag{3}$$

for a first-order desorption process. eq 3 is solved using an experimental TPD spectrum (typically the 1 ML) and an assumed constant prefactor (ν) to obtain an $E_{\mathrm{Des}}(\theta)$ curve. The Polanyi−Wigner eq (eq 1) is numerically integrated using this $E_{\mathrm{Des}}(\theta)$ curve and the assumed prefactor to generate a set of submonolayer TPD spectra. The difference between the experimental and simulated spectra for the entire set is used to calculate a chi square error. The process is repeated using the prefactor as a variational parameter to find the value that best fits the experimental data set.

Before implementing the inversion method, it is possible to obtain estimates of the desorption parameters. One approach is to observe that the benzene TPD spectra have classic first-order desorption lineshapes. In this case, eq 1 can be rearranged to give,

$$\ln\left(\frac{\frac{d\theta}{dT}}{\theta}\right) = \frac{-E_{\mathrm{Des}}}{RT} + \ln(\nu) \tag{4}$$

for n and β equal to 1. Figure 5 is an Arrhenius plot of $(d\theta/dT)/\theta$ for benzene TPD spectra with initial coverages of 0.33, 0.44, 0.55, 0.66, 0.77, and 0.88 ML (from Figure 1). The TPD spectra (plotted to near the desorption peak) nearly align onto a single curve which is consistent with a first-order desorption mechanism. The value of E_{Des} and ν can be obtained from the slope and intercept respectively of a line fit to the curve (see eq 4). The dashed line in Figure 5 is an Arrhenius fit to the 0.88 ML curve which yielded an activation energy of 54.5 ± 2 kJ/mol and a prefactor of $1.0 \times 10^{17\pm1}$ s^{-1}.

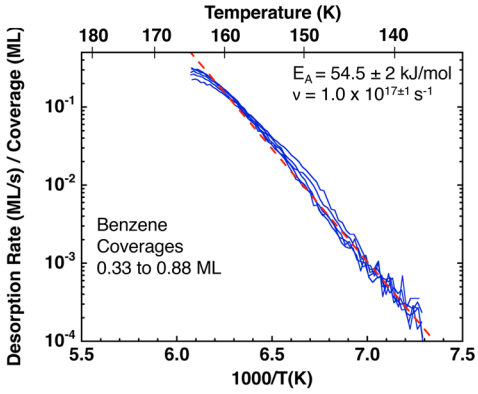

Figure 5. Arrhenius plot of the desorption rate (ML/s) divided by the coverage (ML) for benzene TPD spectra with initial coverages of 0.33, 0.44, 0.55, 0.66, 0.77, and 0.88 ML (from Figure 1). The dashed line is an Arrhenius fit to the 0.88 ML curve which yielded an activation energy of 54.5 ± 2 kJ/mol and a prefactor of $1.0 \times 10^{17\pm1}$ s^{-1}.

Another method for estimating the prefactor is to invert the submonolayer coverages in addition to the 1 ML spectrum. The inversion of all the submonolayer spectra is not necessary for the inversion procedure (described below) but it is useful to estimate the range of potential prefactors. Figure 6 displays the

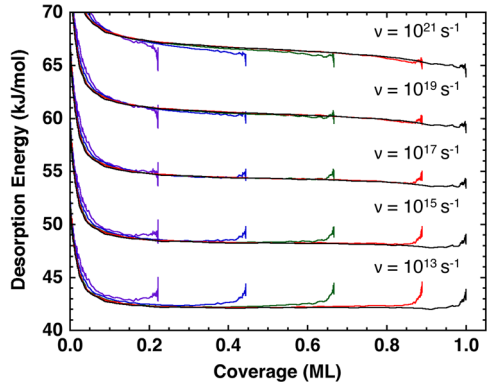

Figure 6. Coverage dependent desorption energy curves obtained by inverting the 0.22, 0.44, 0.66, 0.88, and 1.0 ML benzene TPD spectra in Figure 1 using assumed prefactors of 10^{13}, 10^{15}, 10^{17}, 10^{19}, and 10^{21} s^{-1}.

$E_{\mathrm{Des}}(\theta)$ curves obtained from selected benzene TPD spectra with initial coverages from 0.22 to 1.0 ML using prefactors of 10^{13}, 10^{15}, 10^{17}, 10^{19}, and 10^{21} s^{-1}. For prefactors of 10^{13} s^{-1} and 10^{15} s^{-1} the $E_{\mathrm{Des}}(\theta)$ curves do not align on a single curve but instead veer upward at higher coverages. The $E_{\mathrm{Des}}(\theta)$ curves for a prefactor of 10^{21} s^{-1} also do not align on a single curve but in this case veer downward at higher coverages. The best alignment is obtained with a prefactor of 10^{17} s^{-1}. The alignment of the inverted TPD spectra onto a single curve means that the desorption energy depends only on the coverage at the time of desorption. Although qualitative, the results in Figure 6 predict that the prefactor is close to 10^{17} s^{-1}.

The full inversion procedure is illustrated in Figure 7. The first step is to calculate an $E_{\mathrm{Des}}(\theta)$ for the 1 ML TPD spectrum for a given prefactor (like those displayed in Figure 6). The Polyani-Wigner eq (eq 1) is integrated using this $E_{\mathrm{Des}}(\theta)$ curve and corresponding prefactor to simulate a set of submonolayer coverage TPD spectra. Figure 7a displays a set of simulated TPD spectra (black lines) generated for an assumed prefactor of 10^{17} s^{-1}. Also plotted are the corresponding experimental (open blue circles) TPD spectra. The χ^2 error is calculated from the difference between the set of simulated and experimental spectra. The process is repeated with various prefactors. Figure 7b is a plot of the χ^2 error (solid red circles) versus the log of the prefactor obtained from simulations using prefactors of 10^{13}, 10^{15}, 10^{17}, 10^{19}, and 10^{21} s^{-1}. The dashed line is a quadratic fit to the data and yields a minimum at ~17.1 ($\nu = 1.3 \times 10^{17}$ s^{-1}). The minimum is close to the 10^{17} s^{-1} prefactor although the fit curve shows that the χ^2 error for simulations using prefactors of 10^{16} s^{-1} and 10^{18} s^{-1} would only be slightly larger.

Figure 8 displays the $E_{\mathrm{Des}}(\theta)$ curves obtained using prefactors of 10^{16} (blue line), 10^{17} (black line), and 10^{18} s^{-1} (red line). The curves are relatively flat over most of the coverage range with an increase in E_{Des} at coverages below ~0.05 ML. The relatively flat curves from 0.05 to 1.0 ML indicates the desorption energy is largely coverage independent. The increase in E_{Des} below 0.05 ML could be due to adsorption on a small amount of higher energy binding sites, i.e., defects. The desorption energy at a coverage of 0.5 ML (vertical dashed

DOI: 10.1021/acs.jpcb.7b05102
J. Phys. Chem. B 2018, 122, 587−594

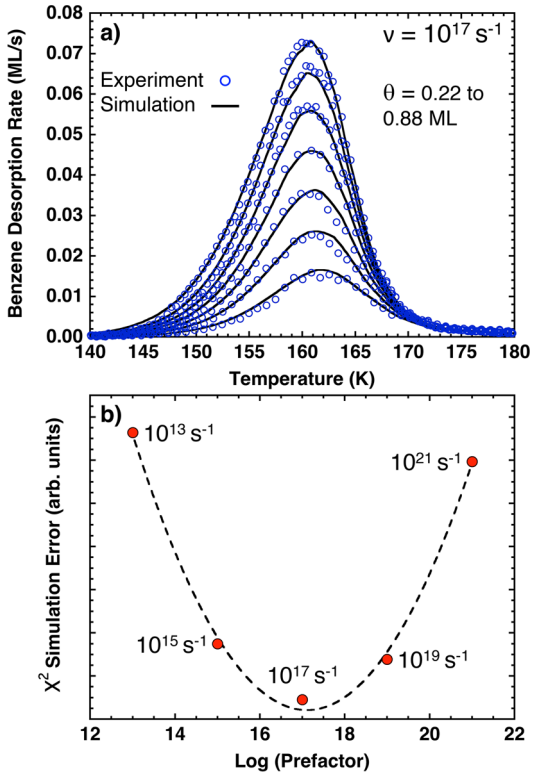

Figure 7. (a) Comparison of benzene TPD experiments (blue open circles) and simulations (black curves). The simulations used a coverage dependent desorption energy curve obtained by inverting the 1.0 ML benzene TPD spectrum using a prefactor of 10^{17} s^{-1}. (b) The total chi square error (solid circles) between the experimental and simulated TPD spectra for all initial coverages versus the log of the prefactor used in the inversion analysis. The dashed line is a quadratic fit to the chi square error points which yields a minimum at ~17.1 (ν = 1.3 × 10^{17} s^{-1}).

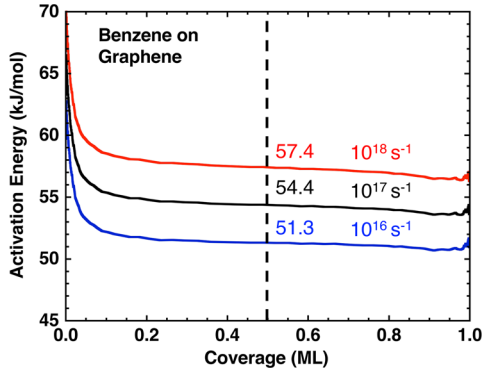

Figure 8. Coverage-dependent binding energy curves for benzene on graphene covered Pt(111) obtained by inversion of the 1 ML TPD spectrum in Figure 1 using prefactors of 10^{16} (blue), 10^{17} (black), and 10^{18} s^{-1} (red). The vertical dashed line is at a coverage of 0.5 ML which gives desorption energies of 51.3, 54.4, and 57.4 kJ/mol for prefactors of 10^{16}, 10^{17}, and 10^{18} s^{-1}, respectively.

line) for the three prefactors 10^{16}, 10^{17}, and 10^{18} s^{-1} is 51.3, 54.4, and 57.4 kJ/mol, respectively. This plot shows that the desorption activation energy of benzene from graphene covered Pt(111) is 54 ± 3 kJ/mol with a prefactor of $10^{17\pm1}$ s^{-1}.

Energetics of Cyclohexane Desorption from Graphene—Zero Order Analysis. The monolayer cyclohexane TPD spectra in Figure 2 have the characteristics of zero-order desorption kinetics (e.g., the alignment of the leading edges and an increase in peak temperature with coverage). For zero-order desorption, the kinetic parameters can be determined from an Arrhenius analysis. Figure 9 is an Arrhenius plot of the

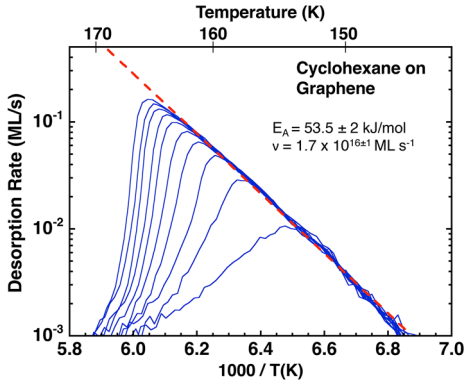

Figure 9. Arrhenius plot of the desorption rate (ML/s) for cyclohexane TPD spectra with initial coverages of 0.1, 0.2, 0.3, 0.4, 0.5, 0.6, 0.7, 0.8, 0.9, and 1.0 ML (from Figure 2). The dashed line is an Arrhenius fit to the 1 ML curve which yielded an activation energy of 53.5 ± 2 kJ/mol and a prefactor of 1.7 × $10^{16\pm1}$ ML s^{-1}.

desorption rate (ML/s) for cyclohexane TPD spectra with initial coverages of 0.1, 0.2, 0.3, 0.4, 0.5, 0.6, 0.7, 0.8, 0.9, and 1.0 ML (from Figure 2). The dashed line is an Arrhenius fit to the 1 ML curve which yielded an activation energy of 53.5 ± 2 kJ/mol and a prefactor of 1.7 × $10^{16\pm1}$ ML s^{-1}.

DISCUSSION AND CONCLUSIONS

The TPD experiments in Figure 1 clearly show that monolayer and submonolayer coverages of benzene desorb from graphene covered Pt(111) with first-order desorption kinetics. Analysis of the TPD spectra using several methods gave consistent values for the desorption parameters. The Arrhenius plot in Figure 5 gave an activation energy of 54.5 ± 2 kJ/mol and a prefactor of 1.0 × $10^{17\pm1}$ s^{-1}. Another method (inversion of the TPD spectra in Figure 6) gave an estimate for the prefactor of ~1.0 × 10^{17} s^{-1}. Finally, the full inversion procedure (Figure 8) yielded a binding energy of 54 ± 3 kJ/mol (at a coverage of 0.5 ML) and a prefactor of $10^{17\pm1}$ s^{-1}. While this prefactor is larger than the typically assumed value of 10^{13} s^{-1}, it is not unusual for large molecules. This is a result of the differences in the molecular degrees of freedom in the adsorbed and desorbed states.[47,51] These differences contribute to the entropy change that occurs during desorption and are reflected in the larger prefactor. Our value of $10^{17\pm1}$ s^{-1} is in good agreement with the prefactor of 9 × $10^{15\pm3}$ s^{-1} estimated by Ulbricht et al. for the desorption of benzene from graphite (HOPG).[33]

There are a few reports of benzene desorption from other carbon-based surfaces. The desorption of benzene from graphite (HOPG) was reported to have a binding energy 48 ± 8 kJ/mol and a prefactor of 9 × $10^{15\pm3}$ s^{-1}.[32,33] This result is in good agreement with our value of 54 ± 3 kJ/mol. The fact that the graphite and graphene covered Pt(111) results are in agreement may mean that either system can be used to study adsorbate interactions with a graphene or graphite surface depending on what is being studied. Only a single desorption energy is reported in the graphite work, so no comparison of the desorption energy coverage dependence is possible.

DOI: 10.1021/acs.jpcb.7b05102
J. Phys. Chem. B 2018, 122, 587−594

In work on graphene covered substrates, desorption energies of 37 kJ/mol (on SiO_2), 39 kJ/mol (on Cu), and 40 kJ/mol (on Ru) at coverages of 0.5 ML were reported.[34,35] These values were obtained using the Redhead equation and an assumed prefactor of 10^{13} s^{-1}. Reanalysis of those data using a prefactor of 10^{17} s^{-1} would increase the binding energies by ~30% and bring them to be closer to our value. In that work, a coverage dependent binding energy is obtained by using the Redhead equation for a series of submonolayer TPD spectra. The results show a much stronger coverage dependence for the desorption energy than ours. For example, on graphene covered Cu, the benzene binding energy varies continuously from 37 kJ/mol at 1.0 ML to 44 kJ/mol at 0.05 ML.[35] This could be either due to strong repulsive interactions between the adsorbates or due to a distribution of higher binding energy defect sites. Our results show a relatively "flat" coverage dependence until coverages less than ~0.05 ML (Figure 8) which would argue against strong long-range repulsive interactions as the explanation. Instead, it is possible that those samples may have more defect sites than ours.

The TPD experiments in Figure 2 show that monolayer and submonolayer coverages of cyclohexane desorb from graphene covered Pt(111) with zero-order desorption kinetics. The Arrhenius plot in Figure 8 gave an activation energy of 53.5 ± 2 kJ/mol and a prefactor of $1.7 \times 10^{16\pm1}$ ML s^{-1}. To our knowledge there have been no experimental publications of the desorption energy of cyclohexane on graphene, however a theoretical paper reports a binding energy of 31 kJ/mol.[52] This value is ~40% lower than our experimental value but this may be due to the calculation being performed on a single graphene layer and not on a graphene covered Pt(111) substrate.

Our prior studies on graphene-covered Pt(111) showed that a wide range of adsorbates (water, methanol, ethanol, Ar, Kr, Xe, N_2, O_2, CO, methane, ethane, and propane) all display zero-order desorption kinetics for monolayer and submonolayer coverages.[29,30] As mentioned above, zero-order desorption kinetics are possible for submonolayer coverages if a two-dimensional equilibrium is established between isolated adsorbates and islands. One might argue that the explanation for the difference between benzene (first-order) and the previous adsorbates (zero-order) is that the prior adsorbates were all smaller (propane being the largest). However, this argument is contradicted by the fact that the cyclohexane exhibits zero-order desorption.

It is also interesting to note that the binding energy is not a determining factor for the desorption order since the values for benzene and cyclohexane are nearly the same, 54 ± 3 kJ/mol and 53.5 ± 2 kJ/mol, respectively. The establishment of a two-dimensional, two-phase equilibrium requires that the surface diffusion rate is fast compared to the desorption rate. We expect this to be the case for both benzene and cyclohexane. For example, the surface diffusion barrier for benzene is calculated to be ~12% of the desorption energy, 5.4 kJ/mol versus 45 kJ/mol, respectively.[19] Assuming that the prefactor for surface diffusion and desorption are the same, at 150 K an average benzene molecule will experience 6×10^{13} diffusive hops prior to desorption.

The obvious difference between benzene and cyclohexane is aromaticity. It has been reported that on graphite (HOPG) the desorption kinetics for benzene, toluene, and naphthalene (all have aromatic rings) are first-order.[33] The transition from zero-order to first-order desorption means that the adsorbate is behaving as a two-dimensional gas without the establishment of an equilibrium with islands. This may mean that the island formation in these aromatic systems is not favored due to the lack of attractive adsorbate interactions. For example, benzene has an order of magnitude larger quadrupole moment compared to cyclohexane (-28.9 C $m^2 \times 10^{-40}$ versus 3.0 C $m^2 \times 10^{-40}$).[53,54] The positively charged outer region of the molecule (the hydrogens) may result in repulsive interactions between coplanar molecules that limit or prohibit the formation of islands. This would account for the observed first-order desorption kinetics. On the other hand, cyclohexane has an order of magnitude smaller quadrupole and the configurational flexibility that may allow for attractive interactions and the formation of two-dimensional islands. This would explain the observation of zero-order desorption kinetics in this case. Future work will further explore how these lateral interactions affect the desorption kinetics of other adsorbates on graphene.

AUTHOR INFORMATION

Corresponding Authors

*Telephone: (509) 371-6156; E-mail: Scott.Smith@PNNL.gov.
*Telephone: (509) 371-6143; E-mail: Bruce.Kay@PNNL.gov.

ORCID

Bruce D. Kay: 0000-0002-8543-2341

Notes

The authors declare no competing financial interest.

ACKNOWLEDGMENTS

This work was supported by the U.S. Department of Energy (DOE), Office of Science, Office of Basic Energy Sciences, Division of Chemical Sciences, Geosciences, and Biosciences. The research was performed using EMSL, a national scientific user facility sponsored by DOE's Office of Biological and Environmental Research and located at Pacific Northwest National Laboratory, which is operated by Battelle operated for the DOE under Contract No. DE-AC05-76RL01830.

REFERENCES

(1) Su, D. S.; Zhang, J.; Frank, B.; Thomas, A.; Wang, X. C.; Paraknowitsch, J.; Schlogl, R. Metal-Free Heterogeneous Catalysis for Sustainable Chemistry. *ChemSusChem* **2010**, 3, 169−180.

(2) Feng, X. F.; Maier, S.; Salmeron, M. Water Splits Epitaxial Graphene and Intercalates. *J. Am. Chem. Soc.* **2012**, *134*, 5662−5668.

(3) Lazar, P.; Karlicky, F.; Jurecka, P.; Kocman, M.; Otyepkova, E.; Safarova, K.; Otyepka, M. Adsorption of Small Organic Molecules on Graphene. *J. Am. Chem. Soc.* **2013**, *135*, 6372−6377.

(4) Fan, X. B.; Zhang, G. L.; Zhang, F. B. Multiple Roles of Graphene in Heterogeneous Catalysis. *Chem. Soc. Rev.* **2015**, *44*, 3023−3035.

(5) Hu, H. W.; Xin, J. H.; Hu, H.; Wang, X. W.; Kong, Y. Y. Metal-Free Graphene-Based Catalyst-Insight into the Catalytic Activity: A Short Review. *Appl. Catal., A* **2015**, *492*, 1−9.

(6) Singh, V.; Joung, D.; Zhai, L.; Das, S.; Khondaker, S. I.; Seal, S. Graphene Based Materials: Past, Present and Future. *Prog. Mater. Sci.* **2011**, *56*, 1178−1271.

(7) Batzill, M. The Surface Science of Graphene: Metal Interfaces, CVD Synthesis, Nanoribbons, Chemical Modifications, and Defects. *Surf. Sci. Rep.* **2012**, *67*, 83−115.

(8) Das, B.; Voggu, R.; Rout, C. S.; Rao, C. N. R. Changes in the Electronic Structure and Properties of Graphene Induced by Molecular Charge-Transfer. *Chem. Commun.* **2008**, 5155−5157.

(9) Feng, X. L.; Marcon, V.; Pisula, W.; Hansen, M. R.; Kirkpatrick, J.; Grozema, F.; Andrienko, D.; Kremer, K.; Mullen, K. Towards High Charge-Carrier Mobilities by Rational Design of the Shape and Periphery of Discotics. *Nat. Mater.* **2009**, *8*, 421−426.

DOI: 10.1021/acs.jpcb.7b05102
J. Phys. Chem. B 2018, 122, 587−594

(10) Li, X. S.; Zhu, Y. W.; Cai, W. W.; Borysiak, M.; Han, B. Y.; Chen, D.; Piner, R. D.; Colombo, L.; Ruoff, R. S. Transfer of Large-Area Graphene Films for High-Performance Transparent Conductive Electrodes. *Nano Lett.* **2009**, *9*, 4359−4363.
(11) Rodriguez-Perez, L.; Herranz, M. A.; Martin, N. The Chemistry of Pristine Graphene. *Chem. Commun.* **2013**, *49*, 3721−3735.
(12) Wu, X.; Vargas, M. C.; Nayak, S.; Lotrich, V.; Scoles, G. Towards Extending the Applicability of Density Functional Theory to Weakly Bound Systems. *J. Chem. Phys.* **2001**, *115*, 8748−8757.
(13) Chakarova-Kack, S. D.; Schroder, E.; Lundqvist, B. I.; Langreth, D. C. Application of Van Der Waals Density Functional to an Extended System: Adsorption of Benzene and Naphthalene on Graphite. *Phys. Rev. Lett.* **2006**, *96*, 146107.
(14) Grimme, S. Do Special Noncovalent Pi-Pi Stacking Interactions Really Exist? *Angew. Chem., Int. Ed.* **2008**, *47*, 3430−3434.
(15) Rochefort, A.; Wuest, J. D. Interaction of Substituted Aromatic Compounds with Graphene. *Langmuir* **2009**, *25*, 210−215.
(16) Tkatchenko, A.; Scheffler, M. Accurate Molecular Van Der Waals Interactions from Ground-State Electron Density and Free-Atom Reference Data. *Phys. Rev. Lett.* **2009**, *102*, 073005.
(17) Al Zahrani, A. Z. First-Principles Study on the Structural and Electronic Properties of Graphene Upon Benzene and Naphthalene Adsorption. *Appl. Surf. Sci.* **2010**, *257*, 807−810.
(18) Bjork, J.; Hanke, F.; Palma, C. A.; Samori, P.; Cecchini, M.; Persson, M. Adsorption of Aromatic and Anti-Aromatic Systems on Graphene through Pi-Pi Stacking. *J. Phys. Chem. Lett.* **2010**, *1*, 3407−3412.
(19) Ershova, O. V.; Lillestolen, T. C.; Bichoutskaia, E. Study of Polycyclic Aromatic Hydrocarbons Adsorbed on Graphene Using Density Functional Theory with Empirical Dispersion Correction. *Phys. Chem. Chem. Phys.* **2010**, *12*, 6483−6491.
(20) Katz, N.; Furman, I.; Biham, O.; Pirronello, V.; Vidali, G. Molecular Hydrogen Formation on Astrophysically Relevant Surfaces. *Astrophys. J.* **1999**, *522*, 305−312.
(21) Pirronello, V.; Liu, C.; Roser, J. E.; Vidali, G. Measurements of Molecular Hydrogen Formation on Carbonaceous Grains. *Astron. Astrophys.* **1999**, *344*, 681−686.
(22) Bolina, A. S.; Wolff, A. J.; Brown, W. A. Reflection Absorption Infrared Spectroscopy and Temperature Programmed Desorption Investigations of the Interaction of Methanol with a Graphite Surface. *J. Chem. Phys.* **2005**, *122*, 044713.
(23) Bolina, A. S.; Wolff, A. J.; Brown, W. A. Reflection Absorption Infrared Spectroscopy and Temperature-Programmed Desorption Studies of the Adsorption and Desorption of Amorphous and Crystalline Water on a Graphite Surface. *J. Phys. Chem. B* **2005**, *109*, 16836−16845.
(24) Bolina, A. S.; Brown, W. A. Studies of Physisorbed Ammonia Overlayers Adsorbed on Graphite. *Surf. Sci.* **2005**, *598*, 45−56.
(25) Brown, W. A.; Bolina, A. S. Fundamental Data on the Desorption of Pure Interstellar Ices. *Mon. Not. R. Astron. Soc.* **2007**, *374*, 1006−1014.
(26) Williams, D. A.; Brown, W. A.; Price, S. D.; Rawlings, J. M. C.; Viti, S. Molecules, Ices and Astronomy. *Astron. Geophys.* **2007**, *48*, 25−34.
(27) Burke, D. J.; Wolff, A. J.; Edridge, J. L.; Brown, W. A. The Adsorption and Desorption of Ethanol Ices from a Model Grain Surface. *J. Chem. Phys.* **2008**, *128*, 104702.
(28) Burke, D. J.; Brown, W. A. Ice in Space: Surface Science Investigations of the Thermal Desorption of Model Interstellar Ices on Dust Grain Analogue Surfaces. *Phys. Chem. Chem. Phys.* **2010**, *12*, 5947−5969.
(29) Smith, R. S.; Matthiesen, J.; Kay, B. D. Desorption Kinetics of Methanol, Ethanol, and Water from Graphene. *J. Phys. Chem. A* **2014**, *118*, 8242−8250.
(30) Smith, R. S.; May, R. A.; Kay, B. D. Desorption Kinetics of Ar, Kr, Xe, N_2, O_2, CO, Methane, Ethane, and Propane from Graphene and Amorphous Solid Water Surfaces. *J. Phys. Chem. B* **2016**, *120*, 1979−1987.
(31) Miliordos, E.; Apra, E.; Xantheas, S. S. Benchmark Theoretical Study of the Pi-Pi Binding Energy in the Benzene Dimer. *J. Phys. Chem. A* **2014**, *118*, 7568−7578.
(32) Zacharia, R.; Ulbricht, H.; Hertel, T. Interlayer Cohesive Energy of Graphite from Thermal Desorption of Polyaromatic Hydrocarbons. *Phys. Rev. B: Condens. Matter Mater. Phys.* **2004**, *69*, 155406.
(33) Ulbricht, H.; Zacharia, R.; Cindir, N.; Hertel, T. Thermal Desorption of Gases and Solvents from Graphite and Carbon Nanotube Surfaces. *Carbon* **2006**, *44*, 2931−2942.
(34) Chakradhar, A.; Trettel, K.; Burghaus, U. Benzene Adsorption on Ru(0001) and Graphene/Ru(0001)-How to Synthesize Epitaxial Graphene without STM or LEED? *Chem. Phys. Lett.* **2013**, *590*, 146−152.
(35) Chakradhar, A.; Sivapragasam, N.; Nayakasinghe, M. T.; Burghaus, U. Adsorption Kinetics of Benzene on Graphene: An Ultrahigh Vacuum Study. *J. Vac. Sci. Technol., A* **2016**, *34*, 021402.
(36) Redhead, P. A. *Vacuum* **1962**, *12*, 203−211.
(37) Kimmel, G. A.; Matthiesen, J.; Baer, M.; Mundy, C. J.; Petrik, N. G.; Smith, R. S.; Dohnalek, Z.; Kay, B. D. No Confinement Needed: Observation of a Metastable Hydrophobic Wetting Two-Layer Ice on Graphene. *J. Am. Chem. Soc.* **2009**, *131*, 12838−12844.
(38) Smith, R. S.; Zubkov, T.; Dohnalek, Z.; Kay, B. D. The Effect of the Incident Collision Energy on the Porosity of Vapor-Deposited Amorphous Solid Water Films. *J. Phys. Chem. B* **2009**, *113*, 4000−4007.
(39) Zubkov, T.; Smith, R. S.; Engstrom, T. R.; Kay, B. D. Adsorption, Desorption, and Diffusion of Nitrogen in a Model Nanoporous Material. I. Surface Limited Desorption Kinetics in Amorphous Solid Water. *J. Chem. Phys.* **2007**, *127*, 184707.
(40) Wu, K. J.; Peterson, L. D.; Elliott, G. S.; Kevan, S. D. Time-Resolved Electron-Energy Loss Spectroscopy Study of Water Desorption from Ag(011). *J. Chem. Phys.* **1989**, *91*, 7964−7971.
(41) Kimmel, G. A.; Persson, M.; Dohnalek, Z.; Kay, B. D. Temperature Independent Physisorption Kinetics and Adsorbate Layer Compression for Ar Adsorbed on Pt(111). *J. Chem. Phys.* **2003**, *119*, 6776−6783.
(42) Daschbach, J. L.; Peden, B. M.; Smith, R. S.; Kay, B. D. *J. Chem. Phys.* **2004**, *120*, 1516−1523.
(43) Smith, R. S.; Petrik, N. G.; Kimmel, G. A.; Kay, B. D. Thermal and Nonthermal Physiochemical Processes in Nanoscale Films of Amorphous Solid Water. *Acc. Chem. Res.* **2012**, *45*, 33−42.
(44) May, R. A.; Smith, R. S.; Kay, B. D. Mobility of Supercooled Liquid Toluene, Ethylbenzene, and Benzene near Their Glass Transition Temperatures Investigated Using Inert Gas Permeation. *J. Phys. Chem. A* **2013**, *117*, 11881−11889.
(45) Masel, R. I. *Principles of Adsorption and Reaction on Solid Surfaces*; Wiley: New York, 1996.
(46) Tait, S. L.; Dohnalek, Z.; Campbell, C. T.; Kay, B. D. n-Alkanes on MgO(100). I. Coverage-Dependent Desorption Kinetics of n-Butane. *J. Chem. Phys.* **2005**, *122*, 164707.
(47) Tait, S. L.; Dohnalek, Z.; Campbell, C. T.; Kay, B. D. n-Alkanes on MgO(100). II. Chain Length Dependence of Kinetic Desorption Parameters for Small n-Alkanes. *J. Chem. Phys.* **2005**, *122*, 164708.
(48) Dohnalek, Z.; Kim, J.; Bondarchuk, O.; White, J. M.; Kay, B. D. Physisorption of N_2, O_2, and CO on Fully Oxidized TiO_2(110). *J. Phys. Chem. B* **2006**, *110*, 6229−6235.
(49) Tait, S. L.; Dohnalek, Z.; Campbell, C. T.; Kay, B. D. n-Alkanes on Pt(111) and on C(0001)/Pt(111): Chain Length Dependence of Kinetic Desorption Parameters. *J. Chem. Phys.* **2006**, *125*, 234308.
(50) Smith, R. S.; Li, Z. J.; Dohnalek, Z.; Kay, B. D. Adsorption, Desorption, and Displacement Kinetics of H_2O and CO_2 on Forsterite, Mg_2SiO_4(011). *J. Phys. Chem. C* **2014**, *118*, 29091−29100.
(51) Fichthorn, K. A.; Miron, R. A. Thermal Desorption of Large Molecules from Solid Surfaces. *Phys. Rev. Lett.* **2002**, *89*, 196103.
(52) Sayin, C. S.; Toffoli, D.; Ustunel, H. Covalent and Noncovalent Functionalization of Pristine and Defective Graphene by Cyclohexane and Dehydrogenated Derivatives. *Appl. Surf. Sci.* **2015**, *351*, 344−352.
(53) Craven, I. E.; Hesling, M. R.; Laver, D. R.; Lukins, P. B.; Ritchie, G. L. D.; Vrbancich, J. Polarizability Anisotropy, Magnetic-Anisotropy,

DOI: 10.1021/acs.jpcb.7b05102
J. Phys. Chem. B 2018, 122, 587−594

and Quadrupole-Moment of Cyclohexane. *J. Phys. Chem.* **1989**, *93*, 627−631.
(54) Trudell, J. R. Contributions of Dipole Moments, Quadrupole Moments, and Molecular Polarizabilities to the Anesthetic Potency of Fluorobenzenes. *Biophys. Chem.* **1998**, *73*, 7−11.

DOI: 10.1021/acs.jpcb.7b05102
J. Phys. Chem. B 2018, 122, 587−594